

Enhanced spin-orbit torque efficiency in $Pt_{100-x}Ni_x$ alloy based magnetic bilayer

Congli He(何聪丽), Qingqiang Chen(陈庆强), Shipeng Shen(申世鹏), Jinwu Wei(魏晋武), Hongjun Xu(许洪军), Yunchi Zhao(赵云驰), Guoqiang Yu(于国强), and Shouguo Wang(王守国)

Citation: Chin. Phys. B, 2021, 30 (**3**): 037503. DOI: 10.1088/1674-1056/abe3f4
Journal homepage: http://cpb.iphy.ac.cn; http://iopscience.iop.org/cpb

What follows is a list of articles you may be interested in

Field-induced N\'eel vector bi-reorientation of a ferrimagnetic insulator in the vicinity of compensation temperature

Peng Wang(王鹏), Hui Zhao(赵辉), Zhongzhi Luan(栾仲智), Siyu Xia(夏思宇), Tao Feng(丰韬), and Lifan Zhou(周礼繁)

Chin. Phys. B, 2021, 30 (**2**): 027501. DOI: 10.1088/1674-1056/abbbef

Magnetization reorientation induced by spin–orbit torque in YIG/Pt bilayers

Ying-Yi Tian(田颖异), Shuan-Hu Wang(王拴虎), Gang Li(李刚), Hao Li(李豪), Shu-Qin Li(李书琴), Yang Zhao(赵阳), Xiao-Min Cui(崔晓敏), Jian-Yuan Wang(王建元), Lv-Kuan Zou(邹吕宽), and Ke-Xin Jin(金克新)

Chin. Phys. B, 2020, 29 (**11**): 117504. DOI: 10.1088/1674-1056/abb666

Anomalous Hall effect in ferromagnetic Weyl semimetal candidate $Zr_{1-x}V_xCo_{1.6}Sn$

Guangqiang Wang(王光强), Zhanghao Sun(孙彰昊), Xinyu Si(司鑫宇), Shuang Jia(贾爽)

Chin. Phys. B, 2020, 29 (**7**): 077503. DOI: 10.1088/1674-1056/ab8da8

Magnetic field enhanced single particle tunneling in MoS_2-superconductor vertical Josephson junction

Wen-Zheng Xu(徐文正), Lai-Xiang Qin(秦来香), Xing-Guo Ye(叶兴国), Fang Lin(林芳), Da-Peng Yu(俞大鹏), Zhi-Min Liao(廖志敏)

Chin. Phys. B, 2020, 29 (**5**): 057502. DOI: 10.1088/1674-1056/ab8209

Magnetic properties of AlN monolayer doped with group 1A or 2A nonmagnetic element: First-principles study

Ruilin Han(韩瑞林), Xiaoyang Chen(陈晓阳), Yu Yan(闫羽)

Chin. Phys. B, 2017, 26 (**9**): 097503. DOI: 10.1088/1674-1056/26/9/097503

RAPID COMMUNICATION

Enhanced spin–orbit torque efficiency in $Pt_{100-x}Ni_x$ alloy based magnetic bilayer*

Congli He(何聪丽)[1,†], Qingqiang Chen(陈庆强)[1,†], Shipeng Shen(申世鹏)[1], Jinwu Wei(魏晋武)[2], Hongjun Xu(许洪军)[2], Yunchi Zhao(赵云驰)[2], Guoqiang Yu(于国强)[2], and Shouguo Wang(王守国)[1,‡]

[1] *Institute of Advanced Materials, Beijing Normal University, Beijing* 100875, *China*

[2] *Beijing National Laboratory for Condensed Matter Physics, Institute of Physics, Chinese Academy of Sciences, Beijing* 100190, *China*

(Received 13 January 2021; revised manuscript received 5 February 2021; accepted manuscript online 8 February 2021)

The binary alloy/ferromagnetic metal heterostructure has drawn extensive attention in the research field of spin–orbit torque (SOT) due to the potential enhancement of SOT efficiency via composition engineering. In this work, the magnetic properties and SOT efficiency in the $Pt_{100-x}Ni_x/Ni_{78}Fe_{22}$ bilayers were investigated via the spin-torque ferromagnetic resonance (ST-FMR) technique. The effective magnetic anisotropy field and effective damping constant extracted by analyzing the ST-FMR spectra show a weak dependence on the Ni concentration. The effective spin-mixing conductance of $8.40 \times 10^{14}\ \Omega^{-1} \cdot m^{-2}$ and the interfacial spin transparency T_{in} of 0.59 were obtained for the sample of $Pt_{70}Ni_{30}$/NiFe bilayer. More interestingly, the SOT efficiency that is carefully extracted from the angular dependence of ST-FMR spectra shows a nonmonotonic dependence on the Ni concentration, which reaches the maximum at $x = 18$. The enhancement of the SOT efficiency by alloying the Ni with Pt shows potential in lowering the critical switching current. Moreover, alloying relatively cheaper Ni with Pt may promote to reduce the cost of SOT devices.

Keywords: spin-orbit torque, magnetic doping, spin-torque ferromagnetic resonance

PACS: 75.47.−m, 85.75.−d, 71.70.Ej **DOI:** 10.1088/1674-1056/abe3f4

Spin–orbit torque (SOT) has been widely employed for driving magnetization switching,[1–8] magnetization oscillation,[9–12] domain wall motion,[13–15] and skyrmion motion,[16–19] exhibiting promising potentials in spintronic device applications. A typical SOT sample has a bilayer structure consisting of heavy metal (HM)/ferromagnetic metal (FM). In general, the HMs are chosen from 5d elements, such as Ta, W, and Pt.[1–7,9–21] When passing an electrical current in the HM/FM, it generates an out-of-plane spin current due to spin Hall effect and/or Rashba effect. The spin current diffuses into the adjacent FM layer and exerts torques, i.e., the SOTs, acting on the magnetization of FM. To reduce the electrical current density for magnetization manipulation and hence lower the power consumption, it is essential to enhance the SOT efficiency (ξ_{DL}), which has become one important goal in the study and application of SOT.

One of the effective methods to enhance the SOT efficiency is alloying light nonmagnetic elements with the commonly employed heavy metals, such as doping Al, Hf, Au, Cu into Pt,[22–26] doping Cu into Ta,[27] and doping oxygen into W.[28] The enhancement of SOT efficiency via alloying has been believed to be related to the increased resistivity (ρ_{HM}) of the heavy metal if the SOT is originated from the spin Hall effect and the intrinsic band structure effect is dominant. This is because ξ_{DL} can be expressed as $\xi_{DL} = T_{in}\frac{2e}{\hbar}\sigma_{SH}^{intri}\rho_{HM}$, where σ_{SH} is the spin Hall conductivity,[23,29,30] and thereby ξ_{DL} can be enhanced by increasing the ρ_{HM} if the σ_{SH} is not degraded and the spin transparency T_{in} at the interface keeps almost unchanged.[23] More recently, it has been reported that doping magnetic element Fe into heavy mental Pt can also enhance the SOT efficiency.[31] The enhancement reaches the maximum near the Curie temperature, which is thereby attributed to the spin fluctuations. Other attempts have been made on the Ni-doped alloys,[32–34] which also exhibit large SOT efficiency even in the absence of heavy metal elements. The observation of large SOT efficiency due to Ni doping is in consistent with the previous tight-binding model calculations.[35,36] These studies motivate us to further explore the enhancement of SOT efficiency by alloying the Ni with other materials, in particular the heavy metals.

In this work, the magnetic properties and SOT efficiency in $Pt_{100-x}Ni_x$/ $Ni_{78}Fe_{22}$(NiFe) bilayers were studied by spin-torque ferromagnetic resonance (ST-FMR) technique.[37–40] The effective anisotropy field and effective damping constant (α_{eff}) were obtained via analyzing the ST-FMR spectra. The effective spin-mixing conductance and the interfacial spin

*Project supported by the National Natural Science Foundation of China (Grant Nos. 51901025 and 51625101), the Fundamental Research Funds for the Central Universities, China (Grant No. 310421101), and the Beijing Natural Science Foundation, China (Grant No. Z190007).

†These authors contributed equally.

‡Corresponding author. E-mail: sgwang@bnu.edu.cn

© 2021 Chinese Physical Society and IOP Publishing Ltd

transparency were further extracted. The results show that the SOT efficiency can be enhanced by doping the magnetic Ni into Pt, and it reaches the maximum value when $x = 18$. These results may be useful for designing and developing SOT-driven spintronic devices.

Two series of multilayer stacks were prepared: (I) $Pt_{100-x}Ni_x$(6)/NiFe(5)/MgO(2)/Pt(2) (thicknesses in nm) with $x = 0$, 6, 12, 18, and 30, respectively; (II) $Pt_{70}Ni_{30}$(6)/NiFe(t)/MgO(2)/Pt(2) with $t = 2$, 3.5, 5, 6.5, and 8, respectively. All the stacks were deposited on thermally oxidized Si substrates by magnetron sputtering tool in a vacuum of less than 5×10^{-8} Torr and at Ar pressure of 3 mTorr at room temperature. The composition of $Pt_{100-x}Ni_x$ was tuned by co-sputtering Pt and Ni under different powers. The multilayers were then patterned into Hall bars and rectangular strips by UV lithography and Ar ion milling for typical four-point resistance measurements and ST-FMR measurements, respectively. The contact electrodes with Cr/Au were used for electrical measurements.

The schematic of the devices for ST-FMR measurements and the coordinates are illustrated in the inset of Fig. 1(a). The details for ST-FMR measurement can be found in our previous work.[37,38,40] The power of the microwave used for this measurement is 13 dBm. Figure 1(a) shows the ST-FMR spectra for the $Pt_{100-x}Ni_x$(6)/NiFe(5) sample with $x = 18$ under the frequency of 9.0 GHz. The results can be well fitted by a sum of symmetric and antisymmetric Lorentzian functions

$$V_{\rm mix} = S\frac{\Delta H^2}{\Delta H^2 + (H_{\rm ext} - H_0)^2} + A\frac{\Delta H(H_{\rm ext} - H_0)}{\Delta H^2 + (H_{\rm ext} - H_0)^2}, \quad (1)$$

where ΔH is the linewidth, H_0 is the resonant magnetic field, S is the symmetric Lorentzian coefficient, and A is the antisymmetric Lorentzian coefficient. Figure 1(b) presents the resonance frequency f as a function of the resonant field $\mu_0 H_0$ for different samples. The results for different samples are quite identical, and they can be well fitted by the Kittel equation $f = (\gamma/2\pi)[\mu_0 H_0(\mu_0 H_0 + 4\pi M_{\rm eff})]^{1/2}$ (γ is the gyromagnetic ratio and μ_0 is the vacuum permeability). The effective magnetization fields ($4\pi M_{\rm eff}$) for different samples are extracted from the fitting,[38] as shown in Fig. 1(d), which exhibit a weak dependence on the Ni concentration. Figure 1(c) shows the frequency dependence of resonance linewidth ΔH for the samples with various Ni concentrations. The results can be linearly fitted by $\Delta H = \Delta H_0 + (2\pi\alpha_{\rm eff}/\gamma)f$, based on which the effective damping constants are thus obtained, as shown in Fig. 1(d). Similar to the effective magnetization field, the effective damping constant also exhibits a weak dependence on the Ni concentration, indicating that the Ni doping does not have an obvious influence on the magnetic properties of the adjacent NiFe layer.

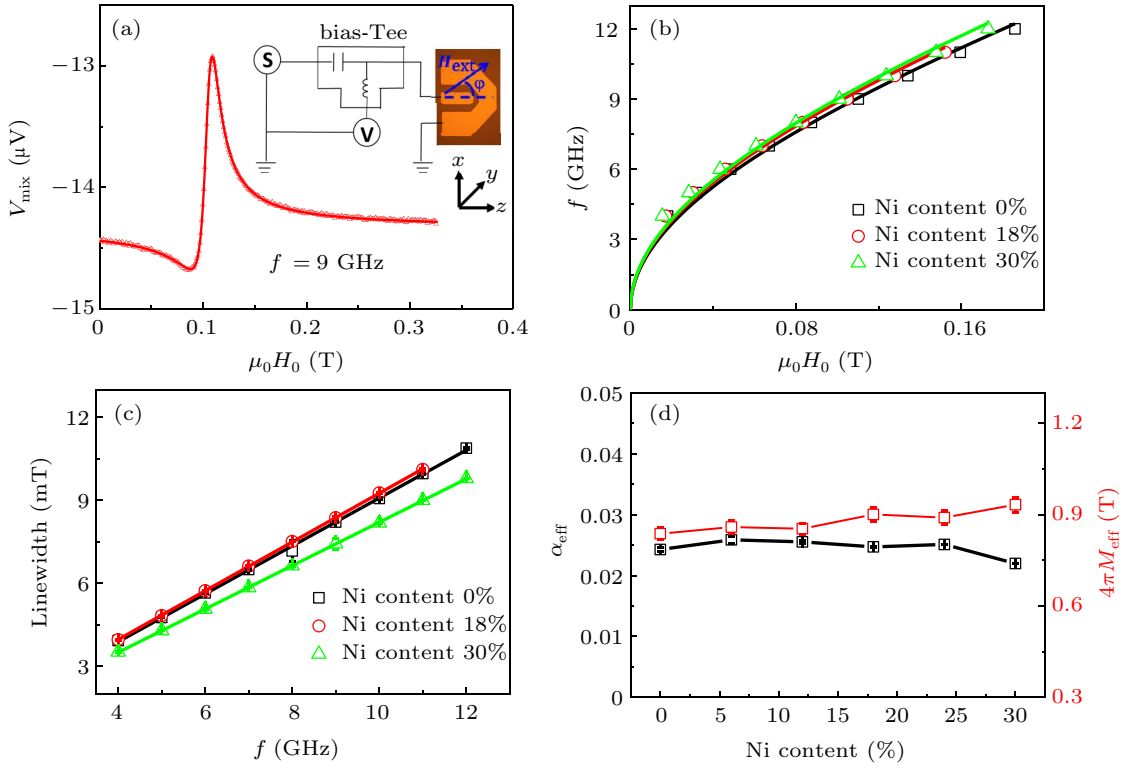


Fig. 1. (a) ST-FMR spectrum for $Pt_{100-x}Ni_x$(6 nm)/NiFe(5 nm)/MgO(2 nm)/Pt(2 nm) with $x = 18$ under the frequency of 9.0 GHz, which is fitted to a Lorentzian function consisting of a symmetric and an antisymmetric Lorentzian component (the solid curves). Inset: schematic of a $Pt_{100-x}Ni_x$/NiFe device for ST-FMR measurements. (b) Resonance frequency f versus the resonant field $\mu_0 H_0$ for $Pt_{100-x}Ni_x$/NiFe devices, which can be well fitted to the Kittel equation. (c) The linewidth as a function of the resonance frequency f, which can be linearly fitted. (d) The effective damping constant $\alpha_{\rm eff}$ determined by the linear fitting, and the effective magnetization fields $4\pi M_{\rm eff}$ for $Pt_{100-x}Ni_x$/NiFe devices with different Ni contents.

The $Pt_{70}Ni_{30}$/NiFe(t) samples with different thicknesses of NiFe layer were also measured for investigating the interfacial spin transmission. Figure 2(a) shows the resonance frequency f as a function of the resonant field $\mu_0 H_0$. These results can also be well fitted by the Kittel equation. Figure 2(b) shows the effective magnetization fields $4\pi M_{\rm eff}$ for the $Pt_{70}Ni_{30}$/NiFe(t) devices, which decrease from 0.910 ± 0.023 T to 0.349 ± 0.004 T as the thickness of the NiFe layer decreases from 8.0 nm to 2.0 nm, reflecting the gradual increasing contribution of the interfacial anisotropy with decreasing thickness. Figure 2(c) shows the linewidth ΔH versus the resonance frequency f for different samples, which allows us to extract the $\alpha_{\rm eff}$ values for different samples. The $\alpha_{\rm eff}$ as a function of $t_{\rm NiFe}$ is given in the inset of Fig. 2(d), which increases from 0.017 to 0.104 as the NiFe thickness decreases from 8.0 nm to 2.0 nm.

Based on the previous studies,[40,41] the damping can be approximately given by

$$\begin{aligned}\alpha_{\rm eff} &= \alpha_{\rm int} + \alpha_{\rm SP} + \alpha_{\rm TMS} \\ &= \alpha_{\rm int} + G_{\rm eff}^{\uparrow\downarrow} \frac{g\mu_{\rm B} h}{4\pi M_{\rm s} e^2} t_{\rm NiFe}^{-1} + \beta_{\rm TMS} t_{\rm NiFe}^{-2}, \end{aligned} \tag{2}$$

where $\alpha_{\rm int}$ and $M_{\rm s}$ are the intrinsic damping and the saturation magnetization of the NiFe layer; g, $\mu_{\rm B}$, h, and e are the gyromagnetic ratio, the Bohr magnetron, the Planck's constant, and the electron charge, respectively. $G_{\rm eff}^{\uparrow\downarrow}$ is the effective spin-mixing conductance, and $\beta_{\rm TMS}$ is a coefficient that depends on the two-magnon scattering (TMS). Figure 2(d) shows the effective damping constant $\alpha_{\rm eff}$ replotted as a function of $t_{\rm NiFe}^{-1}$. In the thick NiFe film region ($t_{\rm NiFe} > 3.5$ nm), $\alpha_{\rm eff}$ approximately shows a linear dependence on $t_{\rm NiFe}^{-1}$, which is the typical behavior of spin pumping effect (SP). However, with the thickness of the NiFe film decreasing ($t_{\rm NiFe} < 3.5$ nm), $\alpha_{\rm eff}$ deviates from the linear fitting obviously and follows a quadratic dependence. Therefore, the TMS effect must be taken into account for understanding the results, especially in the thin NiFe layer region. By fitting the results to Eq. (2), the effective spin-mixing conductance $G_{\rm eff}^{\uparrow\downarrow}$ is obtained to be $8.40 \times 10^{14}\ \Omega^{-1} \cdot {\rm m}^{-2}$ for the $Pt_{70}Ni_{30}$/NiFe(t), which is comparable with that of the previously reported Pt/NiFe bilayer without doping.[42] The interfacial spin transparency $T_{\rm in}$ is another important parameter since it directly reflects the spin transmission efficiency at the interface. $T_{\rm in}$ could be estimated by[43]

$$T_{\rm in} = 2G_{\rm eff}^{\uparrow\downarrow} \tanh\left(\frac{t_{\rm HM}}{2\lambda_{\rm HM}}\right) \Big/ \left[\frac{1}{\rho_{\rm HM}\lambda_{\rm HM}} + 2G_{\rm eff}^{\uparrow\downarrow} \coth\left(\frac{t_{\rm HM}}{\lambda_{\rm HM}}\right)\right]. \tag{3}$$

Here, $t_{\rm HM}$, $\lambda_{\rm HM}$, and $\rho_{\rm HM}$ are the thickness, spin-diffusion length, and resistivity of the HM layer (here is the $Pt_{70}Ni_{30}$ layer), respectively. We note that the spin diffusion length of pure Pt ($\lambda_{\rm Pt} = 1.9$ nm) is used for estimating the interfacial spin transparency.[25] $T_{\rm in} \approx 0.59$ was obtained for the $Pt_{70}Ni_{30}$/NiFe interface.

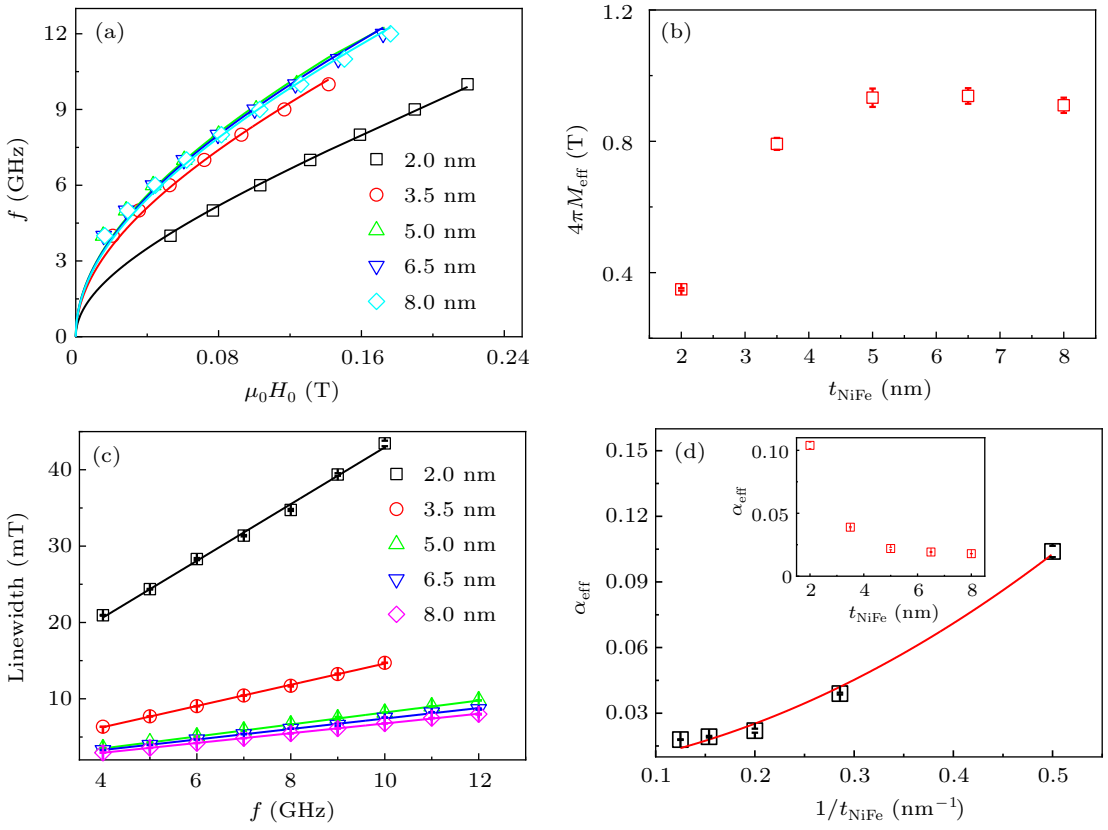


Fig. 2. (a) Resonance frequency f as a function of the resonant field $\mu_0 H_0$ for $Pt_{70}Ni_{30}$/NiFe devices with different thicknesses of NiFe layer. (b) The effective magnetization fields $4\pi M_{\rm eff}$ for $Pt_{70}Ni_{30}$/NiFe devices plotted as a function of the NiFe thickness. (c) The linewidth ΔH versus the resonance frequency f for $Pt_{70}Ni_{30}$/NiFe devices with different thicknesses of NiFe layer. (d) The effect damping constant $\alpha_{\rm eff}$ plotted as a function of $t_{\rm NiFe}^{-1}$ and fitted by Eq. (2) (the solid curve). Inset: effective damping constant as a function of $t_{\rm NiFe}$.

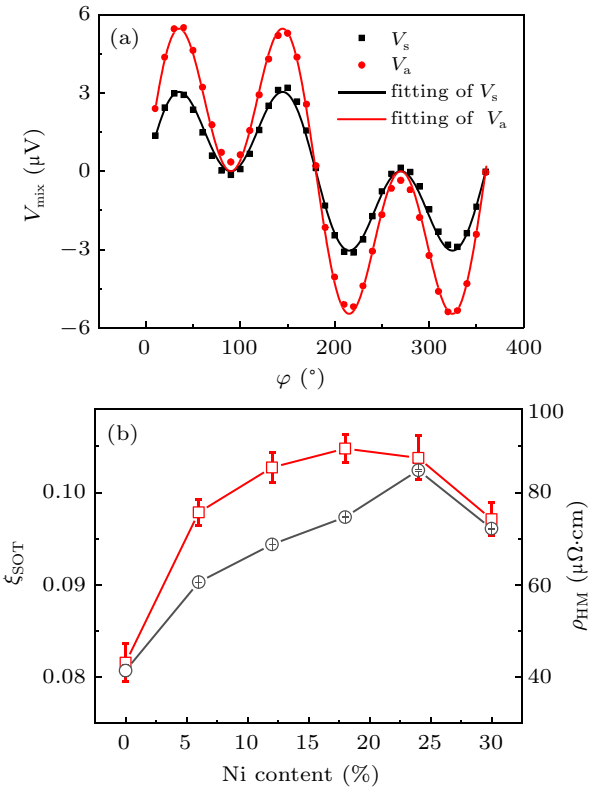


Fig. 3. (a) Angular dependence of symmetric and antisymmetric components for $Pt_{100-x}Ni_x$/NiFe devices with $x = 18$, which are mainly dependent on angle relation of $\cos\phi \sin 2\phi$. (b) The values of SOT efficiency ξ_{SOT} and resistivity ρ_{HM} as a function of Ni content.

Next, we turn to analyze and discuss the SOT efficiency of the samples. The SOT efficiency can be quantitatively determined from the ratio between the symmetric (V_s) and antisymmetric (V_a) components of the resonance curve, which are expressed as[40]

$$V_s = A_s \cos\varphi \sin 2\varphi, \tag{4}$$

$$V_a = A_a \cos\varphi \sin 2\varphi. \tag{5}$$

Figure 3(a) shows the angular dependence of the V_s and V_a components for the $Pt_{100-x}Ni_x$/NiFe devices with $x = 18$, which can be fitted well to $\cos\varphi \sin 2\varphi$. A quantity ξ_{SOT} can be estimated from the V_s/V_a ratio,[44]

$$\xi_{SOT} = \frac{V_s}{V_a}\frac{e}{\hbar}\mu_0 M_s t_{NiFe} t_{HM}\sqrt{1+\frac{4\pi M_{eff}}{\mu_0 H_0}}, \tag{6}$$

where $\hbar$ is the reduced Planck constant. When the field-like torque is quite smaller than the damping-like torque, which is the common situation for the Pt/NiFe bilayer,[45,46] ξ_{SOT} is roughly equal to the damping-like torque efficiency, i.e., $\xi_{SOT} \approx \xi_{DL}$. Figure 3(b) shows the values of ξ_{SOT} extracted by fitting the data and resistivity ρ_{HM} measured by four-point probe measurements as a function of the Ni content. The ξ_{SOT} and ρ_{HM} show quite similar dependence on the Ni concentration, indicating that the SOT efficiency is correlated to the resistivity of $Pt_{100-x}Ni_x$. The correlation is likely because the generated spin current is dominated by the intrinsic mechanism, which is usually believed to be applicable to Pt.[30,47] In this case, ξ_{DL} can be expressed as $\xi_{DL} = T_{in}\frac{2e}{\hbar}\sigma_{SH}^{intri}\rho_{HM}$. By alloying Ni with Pt, the ρ_{HM} is increased, and the σ_{SH} and T_{in} may not be changed,[23] resulting in the increase of ξ_{DL}. According to $\xi_{DL} = \theta_{SH}T_{in} = 0.097 \pm 0.002$ and $T_{in} \approx 0.59$, the corresponding θ_{SH} of $Pt_{70}Ni_{30}$ is further estimated to be 0.164 $\pm$ 0.003, which is comparable with that of $Cu_{100-x}Pt_x$/NiFe system reported in Ref. [26].

In summary, the magnetic properties and SOT efficiency of $Pt_{100-x}Ni_x$/NiFe bilayers were studied by ST-FMR. The effective anisotropy field and effective damping constant exhibit a weak dependence on the Ni concentration. The effective spin-mixing conductance and the interfacial spin transparency were extracted for the $Pt_{70}Ni_{30}$/NiFe. The SOT efficiency can be beneficially enhanced by adding scattering centers to increase the electrical resistivity of the HM, which increases with the Ni concentration and reaches the maximum value when $x = 18$. Our results indicate that the SOT efficiency can be tuned by doping Ni. Considering the low cost of Ni compared to Pt and the enhanced SOT efficiency in $Pt_{100-x}Ni_x$/NiFe, this study may help to reduce the cost of the SOT devices.

References

[1] Miron I M, Garello K, Gaudin G, Zermatten P J, Costache M V, Auffret S, Bandiera S, Rodmacq B, Schuhl A and Gambardella P 2011 *Nature* **476** 189

[2] Liu L Q, Pai C F, Li Y, Tseng H W, Ralph D C and Buhrman R A 2012 *Science* **336** 555

[3] Pai C F, Liu L Q, Li Y, Tseng H W, Ralph D C and Buhrman R A 2012 *Appl. Phys. Lett.* **101** 122404

[4] Yu G Q, Upadhyaya P, Fan Y B, Alzate J G, Jiang W J, Wong K L, Takei S, Bender S A, Chang L T, Jiang Y, Lang M R, Tang J S, Wang Y, Tserkovnyak Y, Amiri P K and Wang K L 2014 *Nat. Nanotechnol.* **9** 548

[5] Qiu X, Shi Z, Fan W, Zhou S and Yang H 2018 *Adv. Mater.* **30** 1705699

[6] Li Y, Edmonds K W, Liu X, Zheng H and Wang K 2019 *Advanced Quantum Technologies* **2** 1800052

[7] Song C, Zhang R, Liao L, Zhou Y, Zhou X, Chen R, You Y, Chen X and Pan F 2020 *Progress in Materials Science* 100761 (in press)

[8] Zheng Z Y, Zhang Y, Zhu D Q, Zhang K, Feng X Q, He Y, Chen L, Zhang Z Z, Liu D J, Zhang Y G, Amiri P K A and Zhao W S 2020 *Chin. Phys. B* **29** 078505

[9] Demidov V E, Urazhdin S, Ulrichs H, Tiberkevich V, Slavin A, Baither D, Schmitz G and Demokritov S O 2012 *Nat. Mater.* **11** 1028

[10] Liu R H, Lim W L and Urazhdin S 2013 *Phys. Rev. Lett.* **110** 147601

[11] Duan Z, Smith A, Yang L, Youngblood B, Lindner J, Demidov V E, Demokritov S O and Krivorotov I N 2014 *Nat. Commun.* **5** 5616

[12] Awad A A, Durrenfeld P, Houshang A, Dvornik M, Iacocca E, Dumas R K and Akerman J 2017 *Nat. Phys.* **13** 292

[13] Emori S, Bauer U, Ahn S M, Martinez E and Beach G S D 2013 *Nat. Mater.* **12** 611

[14] Ryu K S, Thomas L, Yang S H and Parkin S 2013 *Nat. Nanotechnol.* **8** 527

[15] Yu G Q, Upadhyaya P, Wong K L, Jiang W J, Alzate J G, Tang J S, Amiri P K and Wang K L 2014 *Phys. Rev. B* **89** 104421

[16] Jiang W, Upadhyaya P, Zhang W, Yu G, Jungfleisch M, Fradin F, Pearson J, Tserkovnyak Y, Wang K, Heinonen O, te Velthuis S and Hoffmann A 2015 *Science* **349** 283

[17] Yu G Q, Upadhyaya P, Li X, Li W Y, Kim S K, Fan Y B, Wong K L, Tserkovnyak Y, Amiri P K and Wang K L 2016 *Nano Lett.* **16** 1981

[18] Woo S, Litzius K, Kruger B, Im M, Caretta L, Richter K, Mann M, Krone A, Reeve R, Weigand M, Agrawal P, Lemesh I, Mawass M, Fischer P, Klaui M and Beach G 2016 *Nat. Mater.* **15** 501

[19] Yu G, Upadhyaya P, Shao Q, Wu H, Yin G, Li X, He C, Jiang W, Han X, Amiri P K and Wang K L 2017 *Nano Lett.* **17** 261
[20] Shu-Fa Li T Z 2020 *Chin. Phys. B* **29** 087102
[21] Tian Y Y, Wang S H, Li G, Li H, Li S Q, Zhao Y, Cui X M, Wang J Y, Zou L K and Jin K X 2020 *Chin. Phys. B* **29** 117504
[22] Nguyen M H, Zhao M N, Ralph D C and Buhrman R A 2016 *Appl. Phys. Lett.* **108** 242407
[23] Zhu L, Ralph D C and Buhrman R A 2018 *Phys. Rev. Appl.* **10** 031001
[24] Hu C Y and Pai C F 2020 *Advanced Quantum Technologies* **3** 2000024
[25] Obstbaum M, Decker M, Greitner A K, Haertinger M, Meier T N G, Kronseder M, Chadova K, Wimmer S, Kodderitzsch D, Ebert H and Back C H 2016 *Phys. Rev. Lett.* **117** 167204
[26] Shu X, Zhou J, Deng J, Lin W, Yu J, Liu L, Zhou C, Yang P and Chen J 2019 *Phys. Rev. Mater.* **3** 114410
[27] Chen T Y, Wu C T, Yen H W and Pai C F 2017 *Phys. Rev. B* **96** 104434
[28] Demasius K-U, Phung T, Zhang W, Hughes B P, Yang S H, Kellock A, Han W, Pushp A and Parkin S S P 2016 *Nat. Commun.* **7** 10644
[29] Sinova J, Valenzuela S O, Wunderlich J, Back C H and Jungwirth T 2015 *Rev. Mod. Phys.* **87** 1213
[30] Nguyen M H, Ralph D C and Buhrman R A 2016 *Phys. Rev. Lett.* **116** 126601
[31] Ou Y, Ralph D C and Buhrman R A 2018 *Phys. Rev. Lett.* **120** 097203
[32] Keller M W, Gerace K S, Arora M, Delczeg-Czirjak E K, Shaw J M and Silva T J 2019 *Phys. Rev. B* **99** 214411
[33] Varotto S, Cosset-Chéneau M, Grèzes C, Fu Y, Warin P, Brenac A, Jacquot J F, Gambarelli S, Rinaldi C, Baltz V, Attané J P, Vila L and Noël P 2020 *Phys. Rev. Lett.* **125** 267204
[34] Hibino Y, Taniguchi T, Yakushiji K, Fukushima A, Kubota H and Yuasa S 2020 *Phys. Rev. Appl.* **14** 064056
[35] Naito T, Hirashima D S and Kontani H 2010 *Phys. Rev. B* **81** 195111
[36] Jo D, Go D and Lee H W 2018 *Phys. Rev. B* **98** 214405
[37] Liu L Q, Moriyama T, Ralph D C and Buhrman R A 2011 *Phys. Rev. Lett.* **106** 036601
[38] He C L, Navabi A, Shao Q M, Yu G Q, Di Wu D, Zhu W H, Zheng C, Li X, He Q L, Razavi S A, Wong K L, Zhang Z Z, Amiri P K and Wang K L 2016 *Appl. Phys. Lett.* **109** 202404
[39] He C L, Yu G Q, Grezes C, Feng J F, Zhao Z, Razavi S A, Shao Q M, Navabi A, Li X, He Q L, Li M Y, Zhang J, Wong K L, Wei D, Zhang G Y, Han X F, Amiri P K and Wang K L 2018 *Phys. Rev. Appl.* **10** 034067
[40] Wei J W, He C L, Wang X, Xu H J, Liu Y Z, Guang Y, Wan C H, Feng J F, Yu G Q and Han X F 2020 *Phys. Rev. Appl.* **13** 034041
[41] Zhu L J, Ralph D C and Buhrman R A 2019 *Phys. Rev. Lett.* **123** 057203
[42] Ando K, Takahashi S, Ieda J, Kajiwara Y, Nakayama H, Yoshino T, Harii K, Fujikawa Y, Matsuo M, Maekawa S and Saitoh E 2011 *J. Appl. Phys.* **109** 103913
[43] Shao Q M, Tang C, Yu G Q, Navabi A, Wu H, He C L, Li J X, Upadhyaya P, Zhang P, Razavi S A, He Q L, Liu Y W, Yang P, Kim S K, Zheng C, Liu Y Z, Pan L, Lake R K, Han X F, Tserkovnyak Y, Shi J and Wang K L 2018 *Nat. Commun.* **9** 3612
[44] Pai C F, Ou Y X, Vilela-Leao L H, Ralph D C and Buhrman R A 2015 *Phys. Rev. B* **92** 064426
[45] Nan T X, Emori S, Boone C T, Wang X J, Oxholm T M, Jones J G, Howe B M, Brown G J and Sun N X 2015 *Phys. Rev. B* **91** 214416
[46] Wang B, Guo Y H, Han B, Yan Z, Wang T, Yang D Z, Fan X L and Cao J W 2020 *Appl. Phys. Lett.* **116** 222402
[47] Sagasta E, Omori Y, Isasa M, Gradhand M, Hueso L E, Niimi Y, Otani Y and Casanova F 2016 *Phys. Rev. B* **94** 060412